

Ionic Liquids with Carboxylic-Acid-Derived Anions Evaluated as Corrosion Inhibitors under Dynamic Conditions

Natalya V. Likhanova¹, Paulina Arellanes-Lozada², Octavio Olivares-Xometl^{2,*}, Irina V. Lijanovna³, Janette Arriola-Morales², José Carlos Mendoza-Hernández², Grisel Corro⁴

¹ Instituto Mexicano del Petróleo, Programa de Investigación y Posgrado, Eje Central Lázaro Cárdenas No. 152, Col. San Bartolo Atepehuacán, México D.F. 07730, México.

² Facultad de Ingeniería Química, Benemérita Universidad Autónoma de Puebla, Av. San Claudio, Ciudad Universitaria. Col. San Manuel, Puebla, Pue. 72570, México

³ Instituto Politécnico Nacional, CIITEC, Cerrada Cecati S/N, Colonia Santa Catarina, Azcapotzalco, México D.F. 02250, México.

⁴ Instituto de Ciencias, Benemérita Universidad Autónoma de Puebla, 4 sur 104, Puebla 72000, México

*E-mail: oxoctavio@yahoo.com.mx

Received: 11 October 2018 / Accepted: 26 December 2018 / Published: 7 February 2019

The present work deals with the evaluation of three novel ionic liquids (ILs): triethylmethyl ammonium laurate (TAL), triethylmethyl ammonium anthranilate (TAA) and triethylmethyl ammonium oleate (TAO). These compounds were evaluated as corrosion inhibitors (CIs) of API 5L X52 steel in 0.5 M H₂SO₄ by means of electrochemical techniques such as polarization resistance (R_p) and Tafel polarization curves. The electrochemical studies were performed at stationary state ($N_{Re} = 0$) and transitory regime ($N_{Re} = 3375$ and 4500) with concentrations ranging from 10 to 100 ppm. The maximal inhibition efficiencies (IEs) for TAL (78 %) and TAA (73 %) were obtained at 100 ppm and $N_{Re} = 4500$ whereas for TAO (63 %) the IE was reached at $N_{Re} = 3375$. These results confirmed that the IE is also a function of N_{Re} . Furthermore, the Langmuir adsorption isotherm indicated that the IL molecules were adsorbed on the metal surface through a physical phenomenon. From the analysis of the results, a mechanism through which the ILs inhibit the corrosion of API 5L X52 steel in 0.5 M H₂SO₄ was proposed.

Keywords: Electrochemical techniques; Corrosion behaviour; Ionic liquid; Surface analysis.

1. INTRODUCTION

Corrosion is an important research topic for the oil and gas industry, for this phenomenon represents a high percentage of the annual costs in this sector [1]. Cleaning of oil refining equipment,

acidification of oil wells, transportation of hydrocarbons through pipelines, among others, are some of the stages through which corrosion exerts its deleterious effects on this industrial field [1, 2]. The reason for such effects is that carbon steel is one of the main construction materials that is used in this sector not only for its resistance and ductility features, but also for the efficiency-cost ratio [3]. Notwithstanding, this material is highly susceptible to corrosion and because of this, the implementation of preventive measures is paramount to prevent this phenomenon from taking place, thus increasing the useful life of all steel-made parts [4]. One of the most inexpensive and effective corrosion prevention methods is the use of corrosion inhibitors (CIs) which form protection films that delay the metal corrosion rate. The efficiency of CIs depends not only on intrinsic properties such as molecular size, presence of functional groups, steric effects, free electrons, π -conjugated systems and/or heteroatoms [3, 5], but also on external factors like pH, flow rate, pressure, temperature, presence of solids, among others [4]. From the factors mentioned before, the study of the flow rate effect on the CIs is of great scientific interest, for it provides results that are closer to real ones occurring in the oil and gas industry. In this sense, some research works have established a relationship between the flow rate and better CI performance, because the flow rate can increase the mass transfer of the CI molecules toward the metal surface, provoking a positive effect of the CI performance. However, there are opposite theories that state that the hydrodynamic effect can also increase the mass transfer of dissolved metal ions to the electrolyte volume, thus reducing the CI-metal adsorption rate, giving inefficient corrosion protection as a result [4].

For decades, the use of CIs in this sector has been mainly focused on the efficiency that these compounds can provide, nevertheless, factors such as costs, chemical, thermal and dynamic stabilities, environmental regulations and health impact have currently limited the use of conventional CIs, which has encouraged the search of new CI options featuring high inhibition efficiencies (IEs) and low environmental impact [5-7]. Among these compounds, “green” or “environmentally friendly” CIs, as the adjectives suggest, are non-toxic and ecologically accepted chemicals that cause either negligible or null damage, which is the case of ionic liquids (ILs). The IL concept describes a wide group of salts with melting points below 100 °C that are made up of organic cations and organic-inorganic anions that feature unique properties depending on the nature of their ions [8, 9]. Different ILs have been designed as CIs, where phosphonium- [10], imidazolium- [11, 12], ammonium- [13, 14] and pyridinium- [15], among others, derived cations, and anions such as carboxylates [16], halides [17] and sulfonates [18] have been included. More specifically, it has been reported that compounds classified as carboxylic acids and derivatives have displayed good inhibiting activity with IEs up to 99.9 % [19-21]. Although these compounds have not been widely studied, Moussa et al. [20] carried out the study of the effects exerted by aromatic and aliphatic carboxylic acids on the diminution of the corrosion rate using aluminum in acid and basic solutions. Their results suggest that the efficiency of these compounds depends on different factors; in the case of aromatic compounds, it depends mainly on the number and position of the carboxyl group and on the presence of other aromatic ring substituents. As for aliphatic carboxylic acids, the hydrocarbon chain is the most important chemical part that plays a role in the anticorrosive effect, which is directly proportional to the chain length. On the other hand, the study of ILs with quaternary-ammonium-derived cations is of great interest in the CI area, because these compounds display outstanding properties as CIs [8].

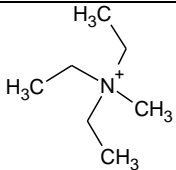
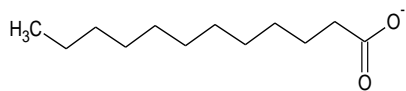
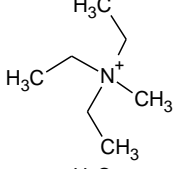
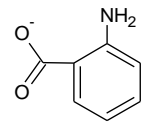
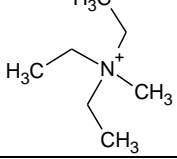
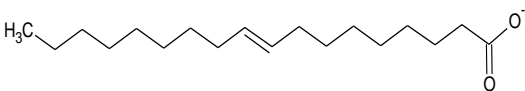
In the present work, the anticorrosive behavior of three novel ILs featuring carboxylic acid and quaternary ammonium derived anions and cations, respectively, was evaluated. The inhibition effect exerted on API 5L X52 steel was studied by using different CI concentrations and 0.5 M H₂SO₄ at stationary and dynamic states. The Tafel polarization curves, polarization resistance (*R_p*) and scanning electron microscopy (SEM) techniques were used to elicit the CI mechanism displayed by the ILs.

2. EXPERIMENTAL

2.1. Test solution

Experiments were performed in a corrosive solution of 0.5 M sulfuric acid, using reagent grade sulfuric acid and deionized water. ILs with carboxylic-acid-derived anions were studied as CIs; Table 1 shows the name, abbreviation and chemical structure of the featured ILs. The concentrations of the ILs were 10, 30, 50, 75 and 100 ppm in 100 mL of corrosive electrolyte for each experiment.

Table 1. Chemical structure of the ILs evaluated as CIs of API 5L X52 steel in 0.5 M H₂SO₄

Abbrv.	Name	Anion	Cation	MW (g/mol)
TAL	Triethylmethyl ammonium laurate			315.6
TAA	Triethylmethyl ammonium anthranilate			252.4
TAO	Triethylmethyl ammonium oleate			398.8

2.2. Materials

The studied material was taken from an API (American Petroleum Institute) 5L X52 steel pipe used for oil and gas transportation. The chemical composition of this material in weight percent is as follows: C (0.08%), Mn (1.06%), Si (0.26%), P (0.019%), S (0.003%), Al (0.0039%), Nb (0.041%), Cs (0.18%), Cr (0.02%), Ni (0.019%), V (0.054%), Ti (0.003%), Ca (0.0002%), B (0.0003%) and Fe (as balance element). The surface of each specimen was wet abraded using SiC sand paper of 320, 600, 100 and 2000 grades. The samples were cleaned with deionized water, rinsed with ethanol and dried carefully to remove the residual water. Both the abrading and cleaning processes were carried out according to the ASTM norms G01-03 and G31-72 [22, 23]. The experiments were performed on totally renewed steel surfaces and in triplicate to ensure the reproducibility of results.

2.3. Electrochemical techniques

The electrochemical tests were performed in a potentiostat/galvanostat AUTOLAB PGSTAT 201 with a three-electrode configuration, using the Autolab Nova software Ver. 2.1.3. Cylindrical specimens of API 5L X52 steel, which have a diameter of 0.7 cm with a protrusion on the top surface coated with Teflon, leaving a working surface of 0.38 cm², were used as rotating disk electrodes. On the other hand, a high-purity platinum foil (99.9%) was used as counter electrode and a saturated calomel electrode (SCE) was the reference electrode, which was placed in a Luggin capillary probe. The rotating system was an Autolab Rotating Disk Electrode (RDE) model 80629 with speed ranging from 100 to 10,000 rpm and 1-rpm resolution. The rotating speed of the RDE was controlled remotely with the corresponding software. All the electrochemical tests were run at stationary and dynamic states at different fluid rates, according to Reynolds numbers (N_{Re}) of 0, 3375 and 4500. The rotational speed was determined by employing the Reynolds equation:

$$N_{Re} = \frac{r^2 \omega}{\nu} \quad (1)$$

where r is the distance from the rotation axis, ω is the rotational speed and ν is the electrolyte kinematic viscosity.

The electrochemical test specimens, under uninhibited and inhibited conditions, were immersed in 0.5 M H₂SO₄ for 15 min in order to obtain a stabilized open circuit potential (E_{OCP}). All the tests were performed in aerated solutions at ambient temperature (25°C ± 3°C). Polarization resistance (R_p) measurements were performed within an interval ranging from $E_{OCP} - 20$ mV to $E_{OCP} + 20$ mV at a scanning rate of 0.166 mV/s. Polarization resistance values were calculated by taking the inverse of the slope of the current potential curve at corrosion potential. The R_p results were reported as overpotential (η) versus current density (i) plots. The η values were calculated by using Equation 2:

$$\eta = E - E_{OCP} \quad (2)$$

During the Tafel polarization test, the samples were polarized from $E_{OCP} - 250$ mV to $E_{OCP} + 250$ mV at a scanning rate of 0.166 mV/s. The extrapolation of the linear cathodic and anodic Tafel curves gave the electrochemical parameters for each test.

2.4. Surface analysis

The images of corroded surfaces and those after inhibitor addition were recorded in a scanning electron microscope (SEM) coupled to a dispersed energy spectrometer (EDX) model JEOL-JSM-6300. The accelerating voltage used to obtain the micrographs was 20 kV at different magnifications. The surface analysis test was performed with the working electrode at $N_{Re} = 4500$ after its immersion in the test solutions (E_{OCP}) in the absence and presence of CIs (concentration of 100 ppm) at ambient temperature (25°C ± 3°C). After 2 h, the samples were taken out, dried and analysed.

3. RESULTS AND DISCUSSION

3.1. Electrochemical results

Figure 1 shows the current density (i , $\mu\text{A cm}^{-2}$) plots as overpotential (η , V/SCE) functions of the API 5L X52 steel surface exposed to the corrosive medium (0.5 M H_2SO_4) with and without the presence of ILs. In these plots, it is observed that in the presence of CI, the slopes of the straight lines are lower than that of the blank, which indicates clearly that the inhibitor changes the energy barrier of the redox reactions, thus controlling the steel corrosion. This result helps establish that the increase in CI concentration favors the polarization resistance and because of this, the corrosion rate is diminished due to the adsorption of CI molecules on the metal surface. Similar figures were obtained for TAL, TAA and TAO at the evaluated N_{Re} .

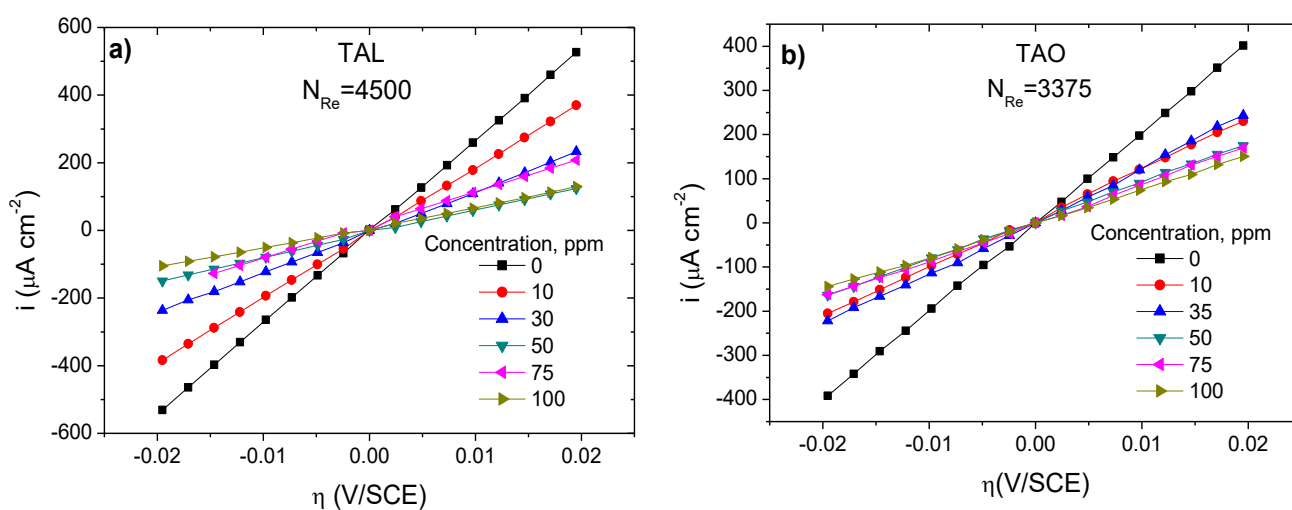
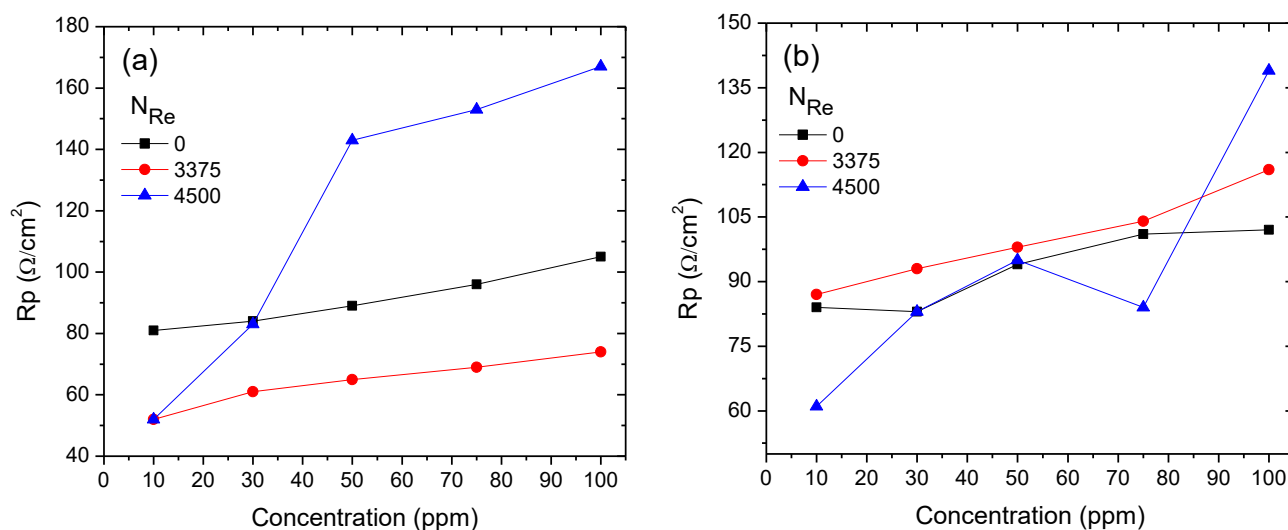


Figure 1. R_p behavior of the ILs: a) TAL at $N_{Re}=4500$ and b) TAO at $N_{Re}=3375$



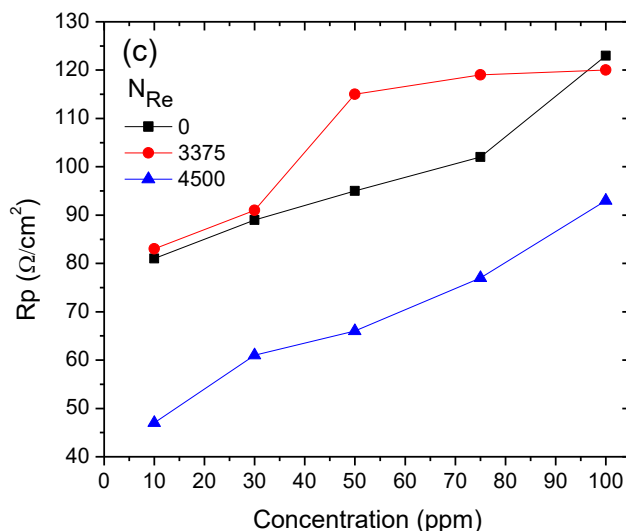


Figure 2. R_p behavior as concentration function of ILs at different N_{Re} : a) TAL, b) TAA and c) TAO

Figure 2 shows the behavior of R_p vs. the CI concentration for the three ILs evaluated as CIs at different N_{Re} . In general, it is observed that the R_p values are increased along with the inhibitor concentration, producing the highest R_p value at 100 ppm for the studied compounds. This fact reveals the occurrence of an inhibition process through two phenomena that are mutually related, which are the current flow and active sites [24]. In this case, the reduction of the corrosion current density was obtained with fewer active sites. However, the attraction forces of the CI molecules toward the steel surface are also affected by the regime change in N_{Re} . Evidence of this is the behavior patterns observed in the TAL, TAA and TAO compounds at $N_{Re} = 3375$ and 4500 whose values are in transition regime ($2300 < N_{Re} < 4000$), where two important phenomena could be possibly considered due to the vortex effect produced by the angular movement of the working electrode [25, 26]. The first one has to do with the shear stress on the steel surface, which reduces the accumulation of corrosion products [27]. In the second one, the vortex favors the attraction of corrosion products and CI molecules. As a result, through fluid momentum effect, both species interact with the steel surface, where the adsorption of TAL and TAA molecules is favored with the increasing N_{Re} . Then, the flux affects the mass transfer coefficient of the involved species (inhibitor molecules and corrosion products) during the formation and dissolution of the inhibitor-corrosion product film, thus affecting the film resistance and steel corrosion rate. Notwithstanding, for TAO, the increase in N_{Re} produced the inhibitor desorption from the steel surface, which allowed suppose that the TAO molecules suffered important changes in their orientation due to the fluid shear stress [28]. Then, the number of active sites on the surface was increased for TAO by passing from $N_{Re} = 3375$ to 4500. The IE obtained by the R_p technique (IE_{Rp} , %) was calculated with Equation (3):

$$IE_{Rp} = \frac{Rp^i - Rp^0}{Rp^i} \times 100 \quad (3)$$

where, Rp^i and Rp^0 are Rp values obtained in the presence and absence of inhibitor. Figure 3 shows the behavior of IE_{Rp} as a function of N_{Re} , where it is clearly observed that IE_{Rp} depends mainly on the inhibitor concentration. Nevertheless, the type of studied regime (N_{Re}) affected the adsorption

phenomena on the inhibitor-surface interphase. By performing the analysis of the maximal IE_{Rp} at 100 ppm of CI, it can be established that at $N_{Re} = 4500$, the most efficient compound was TAL (78 %) whereas at $N_{Re} = 0$ and 3375, the most efficient compound was TAO (49 and 63 %, respectively). The analysis of the structures of the CIs vs. IE_{Rp} evidences the influence of the linearity of the anion structure on the properties of the ILs evaluated as CIs in H_2SO_4 solution; then, the adsorption of the CIs is also related to the anion structure.

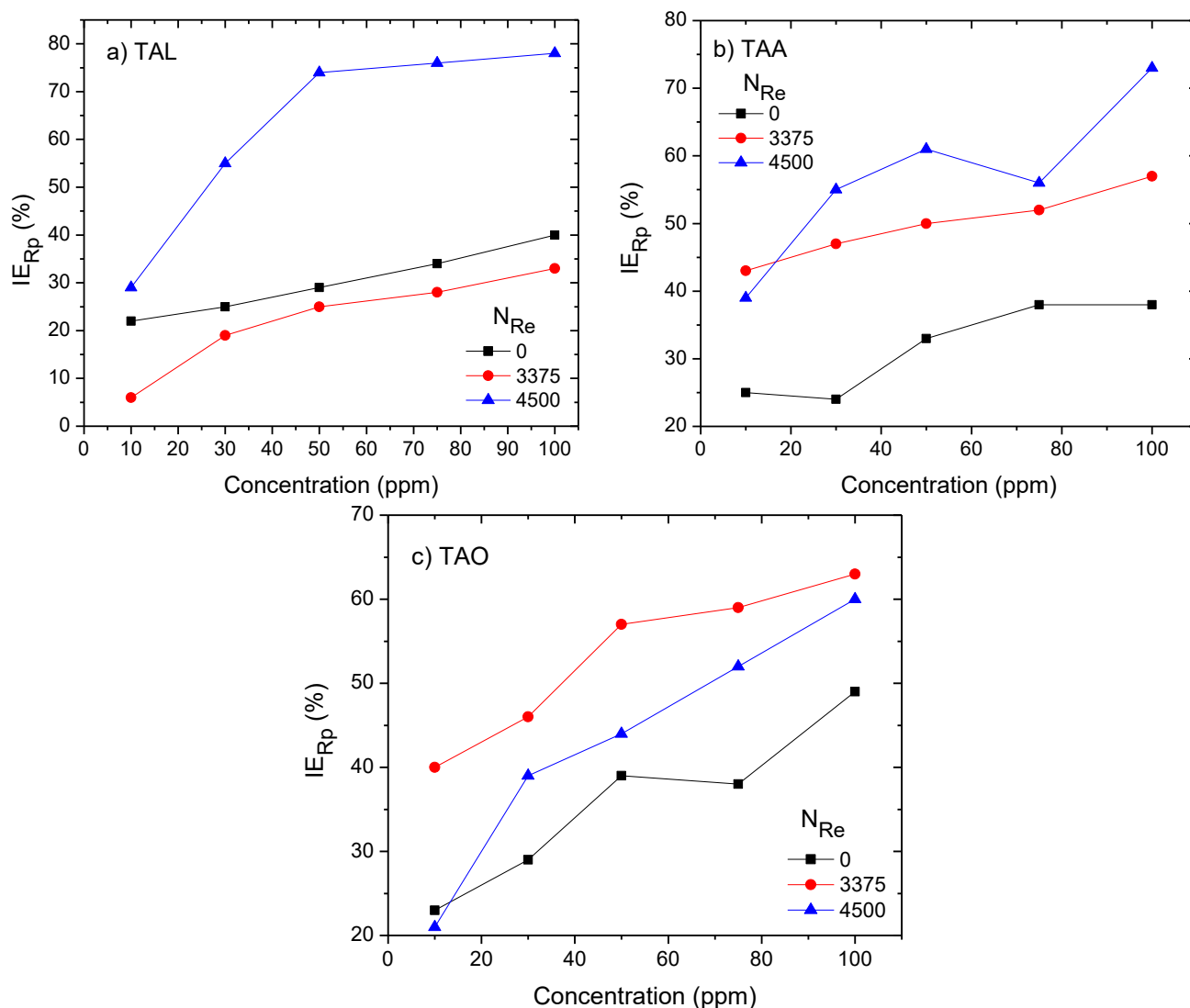


Figure 3. IE_{Rp} behavior as concentration function at different N_{Re} : a) TAL, b) TAA and c) TAO

The Tafel polarization plots at different CI concentrations and $N_{Re} = 0$ for API 5L X52 steel in 0.5 M H_2SO_4 are shown in Figure 4; similar plots were obtained at transition state. In these figures, it is observed that the current intensity of the cathodic and anodic branches in the presence of CI is lower than that observed in the absence of CI, which indicates that the steel dissolution mechanism was modified by an adsorption process of IL molecules on the steel surface. Then, the evaluated inhibitors accomplished the main goal set for CIs, which is to protect the metal surface through a blocking mechanism of active sites as reported elsewhere [29]. Table 2 (a) - (c) reports the electrochemical

parameters obtained through the Tafel technique: slopes of the cathodic and anodic (β_c and β_a) branches, corrosion potential (E_{corr}) and corrosion current density (i_{corr}).

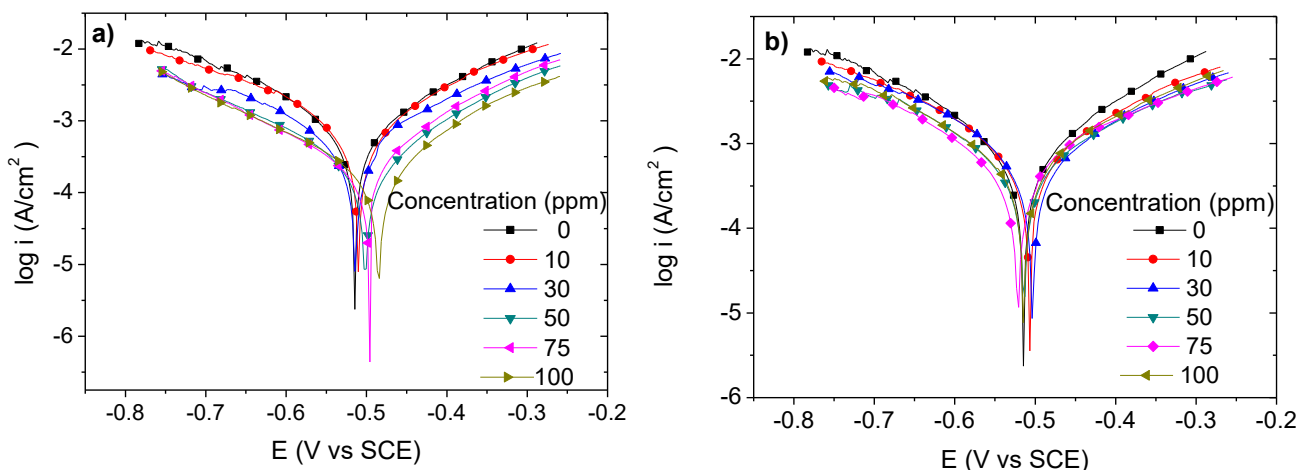


Figure 4. Potentiodynamic polarization curves in 0.5 M H₂SO₄ at $N_{Re} = 0$ and different CI concentrations: a) TAL and b) TAO

Table 2 (a). Corrosion parameters obtained by potentiodynamic polarization in 0.5 M H₂SO₄ at $N_{Re} = 0$

CI	C (ppm)	β_a (mV/dec)	$-\beta_c$ (mV/dec)	$-E_{corr}$ (mV)	i_{corr} ($\mu\text{A}/\text{cm}^2$)	IE_T (%)
-	0	130	43	417	1250	-
TAL	10	124	38	414	988	21
	30	142	52	415	988	21
	50	132	62	420	900	28
	75	153	67	425	813	35
	100	155	71	425	800	36
TAA	10	135	44	423	988	21
	30	143	46	428	975	22
	50	141	41	428	875	30
	75	147	43	427	800	36
	100	112	40	427	813	35
TAO	10	150	43	433	963	23
	30	155	48	431	900	28
	50	149	44	432	800	36
	75	149	43	428	800	36
	100	139	39	436	675	46

Table 2 (b). Corrosion parameters obtained by potentiodynamic polarization in 0.5 M H₂SO₄ at $N_{Re} = 3375$

CI	C (ppm)	β_a (mV/dec)	$-\beta_c$ (mV/dec)	$-E_{corr}$ (mV)	i_{corr} ($\mu\text{A}/\text{cm}^2$)	IE_T (%)
-	0	128	42	431	1380	-
TAL	10	143	463	418	1256	9
	30	119	453	421	1159	16
	50	123	49	422	1021	26
	75	117	52	419	952	31
	100	129	38	419	925	33
TAA	10	135	47	419	800	42
	30	144	53	419	759	45
	50	122	37	419	718	48
	75	129	39	413	690	50
	100	130	41	417	621	55
TAO	10	141	50	433	869	37
	30	151	48	436	773	44
	50	169	53	433	580	58
	75	155	45	433	621	55
	100	127	36	426	538	61

Table 2 (c). Corrosion parameters obtained by potentiodynamic polarization in 0.5 M H₂SO₄ at $N_{Re} = 4500$

CI	C (ppm)	β_a (mV/dec)	$-\beta_c$ (mV/dec)	$-E_{corr}$ (mV)	i_{corr} ($\mu\text{A}/\text{cm}^2$)	IE_T (%)
-	0	193	197	520	4570	-
TAL	10	186	199	515	3290	28
	30	276	239	527	2011	56
	50	192	164	506	1371	70
	75	225	124	500	1325	71
	100	218	155	486	1234	73
TAA	10	235	197	544	2925	36
	30	201	105	509	2194	52
	50	205	187	503	1874	59
	75	180	92	517	2011	56
	100	209	123	482	1188	74
TAO	10	239	253	500	3747	18
	30	218	232	505	2833	38
	50	272	185	512	2605	43
	75	180	144	514	2331	49
	100	237	222	514	1874	59

In order to establish the type of corrosion inhibition produced by the ILs, the corrosion potential displacement values (ΔE_{corr}) in the presence of CIs were calculated with Equation (4):

$$\Delta E_{corr} = E_{corr}^i - E_{corr}^0 \tag{4}$$

where E_{corr}^i and E_{corr}^0 are the corrosion potentials with and without inhibitor. Figure 5 shows the ΔE_{corr} vs. concentration at the different N_{Re} values. TAL, TAA and TAO show displacements toward the cathodic and anodic zones, however, at $N_{Re} = 0$, the three compounds displayed a displacement toward the cathodic branch. Similar observations have been reported by performing galvanic corrosion studies as functions of N_{Re} [30].

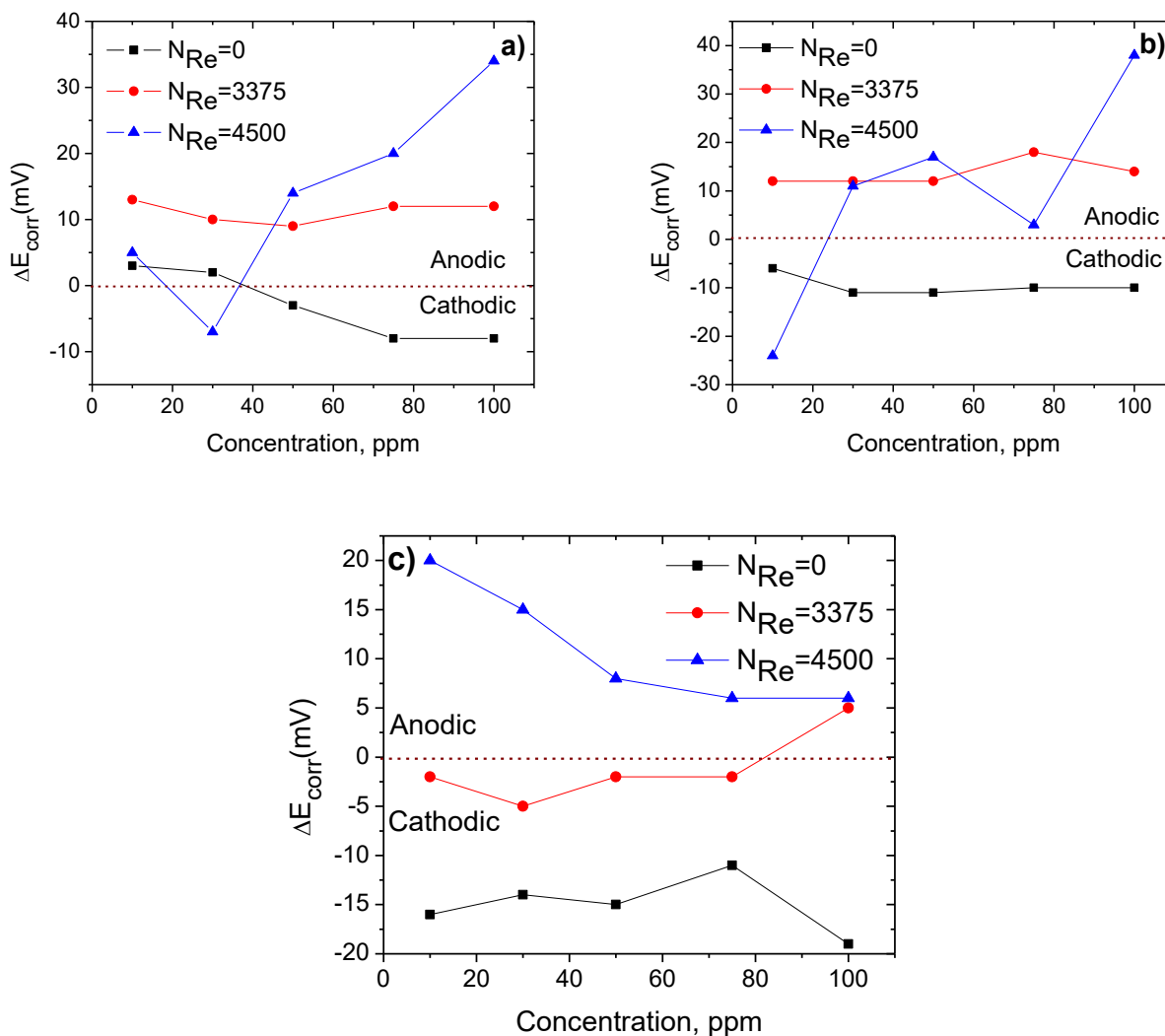


Figure 5. Effect of N_{Re} on the E_{corr} values in 0.5M H_2SO_4 : a) TAL, b) TAA and c) TAO

This observation is important because there are studies that have related the inhibition effect to the ΔE_{corr} value (geometrical blockage by CI molecules, mixed behavior and electro-catalytic effect) [31, 32]. As it can be observed in Figure 5, the obtained displacements are below ± 85 mV, toward the cathodic and anodic zones. Some authors have considered the behavior of ΔE_{corr} as a criterion for classifying CIs [33], and according to this criterion, the ILs evaluated as CIs were classified as mixed-type inhibitors.

The IE obtained by the Tafel curve technique ($IE_T, \%$) was computed as a function of i_{corr} with Equation (5) :

$$IE_T = \frac{i_{corr}^0 - i_{corr}^i}{i_{corr}^0} \times 100 \quad (5)$$

where i_{corr}^0 and i_{corr}^i correspond to the corrosion current intensity in the absence and presence of CI, respectively. In the same table, it is observed that the values of the β_a and β_c slopes do not show a defined concentration trend. In Figure 4, it is observed that the anodic and cathodic slopes are parallel with respect to the curves without CI; then, the ILs did not modify the proton reduction mechanism and iron dissolution, and just the surface geometrical blockage occurred, which diminished the kinetics of reactions.

In Figure 4, the blockage of active sites due to i_{corr} diminution in the presence of CI is corroborated. Then, the presence of CI molecules on the steel surface hinders the free access of corrosive ions to the active sites. Finally, in Table 2 (a) – (c), it is observed that the i_{corr} values are reduced as the CI concentration was increased because the covered surface degree was increased with the adsorption of a higher amount of CI molecules on the steel surface. This phenomenon of adsorption and orientation of CI molecules provokes the diminution of the steel corrosion rate.

In Tables 2 (a) and (b), it is observed that at 100 ppm and $N_{Re} = 0$ and 3375, the most efficient compound was TAO (46 and 61 %) whereas in Table 2 (c) at $N_{Re} = 4500$, TAA (74 %) was the most efficient. According to the aforementioned, the compound with the best CI properties was TAO, confirming that its adsorption on the metal surface was more stable under dynamic conditions. Nevertheless, at transitory regime at higher N_{Re} , the IE_T diminished, because the flow vectors are parallel to the steel surface [34], which originate shear stress that promotes the desorption of molecules, affecting the IE_T . For TAL and TAA at transitory regime, the fluid momentum did not affect their adsorption on the steel surface, producing higher IE_T . On the other hand, it has been reported that CIs containing aromatic rings and pending groups in their chemical structure display, in general, excellent CI properties. TAA has an aromatic ring and an amine group in its chemical structure, however, this potential advantage in combination with the cation did not favor its good performance as CI, because the maximal obtained IE_T was of 74 % at $N_{Re} = 4500$. From the analysis of IE_T , it can be mentioned that the adsorption rate of the ILs on the metal active sites depended mainly on the chemical structure of the anion. Then, when there is high affinity between the CI and the surface, a higher displacement of water molecules by CI molecules on the surface to be protected is achieved, diminishing (i_{corr}) as confirmed in Table 2.

3.2. Adsorption isotherms

The use of adsorption isotherm models has been widely accepted to elicit easily the adsorption type of a CI on metal surfaces. For this reason, it has been established that the CI inhibition efficiency is comparable to the covered surface degree (θ). In the present work, θ was calculated by using Equation (6) and the experimental data were adjusted with the Langmuir adsorption isotherm model (Equation 7):

$$\theta = \left[\frac{IE_{Rp} + IE_T}{2} \right] \left[\frac{1}{100} \right] \quad (6)$$

$$\frac{C}{\theta} = \frac{1}{K_{ads}} + C \quad (7)$$

$$\Delta G_{ads}^0 = -RT \ln(55.5 \times K_{ads}) \tag{8}$$

where K_{ads} is the adsorption equilibrium constant and C is the IL concentration. Figure 6 shows the fitting of the experimental data by using the Langmuir adsorption model for the CIs evaluated at $N_{Re} = 3375$; similar fittings were obtained at $N_{Re} = 0$ and 4500. This fact indicates that the flow regime is an important factor that affects the adsorption rate of the inhibitor molecules. The obtained K_{ads} values and the free energy of adsorption (ΔG_{ads}^0) are reported in Table 3. ΔG_{ads}^0 was calculated with Equation (8), where R is the gas constant and T is the absolute temperature.

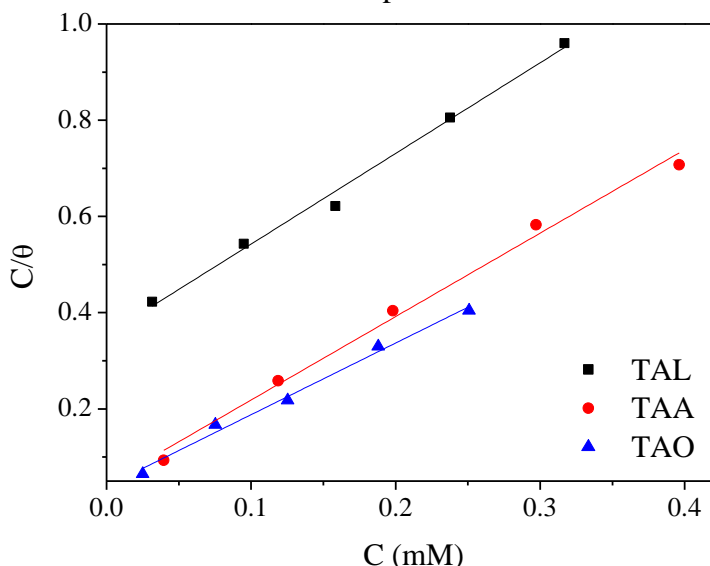


Figure 6. Langmuir adsorption plot of API 5L X52 steel in 0.5 M H₂SO₄ at $N_{Re} = 3375$

Table 3. Thermodynamic parameters of the experimental corrosion system

N_{Re}	CI	R^2	K_{ads} (mmol ⁻¹)	$-\Delta G_{ads}^0$ (kJ mol ⁻¹)
0	TAL	0.960	7.0	31.9
	TAA	0.968	6.9	31.9
	TAO	0.944	10.4	32.9
3375	TAL	0.993	2.8	29.7
	TAA	0.993	22.2	34.8
	TAO	0.991	25.6	35.1
4500	TAL	0.991	14.9	33.8
	TAA	0.946	14.2	33.7
	TAO	0.982	9.7	32.7

The ΔG_{ads}^0 values confirmed that the inhibition process performed by the CIs occurred mainly through a physical and chemical adsorption mechanism, driven by electrostatic attraction forces and donation of

electrons between the surface and inhibitor [12, 35].

3.3. Surface characterization by SEM

Figure 7(a) shows the micrograph of the API 5L X-52 steel surface before being immersed in 0.5 M H₂SO₄, where the typical orientation of lines produced by the surface polishing and the presence of non-metallic inclusions are observed. Figure 7(b) corresponds to the steel surface without inhibitor, which denotes severe surface damage with the corresponding steel mass loss and the presence of low-solubility corrosion products such as szomolnokite, goethite and ferric hydroxide, among others [36, 37].

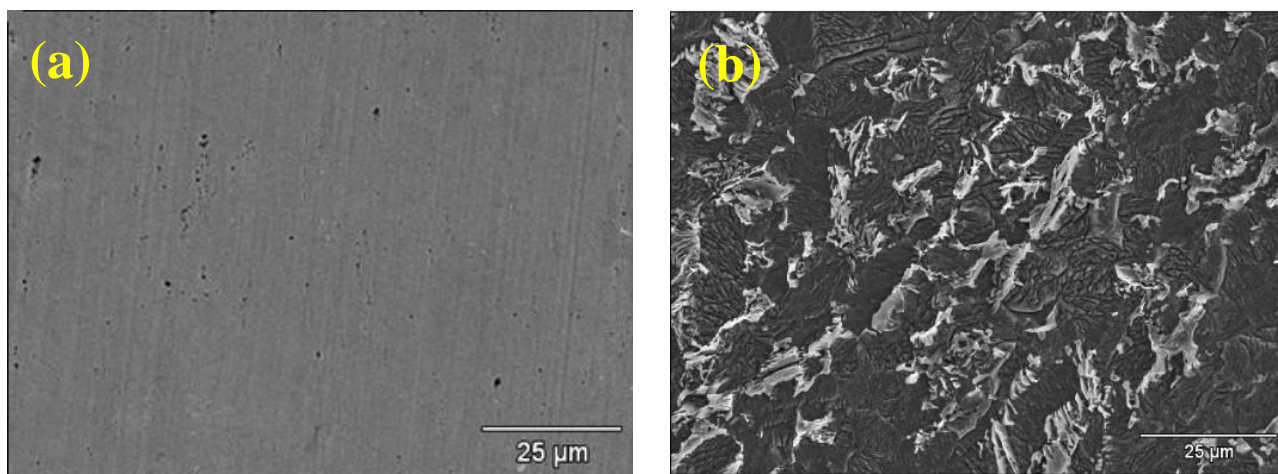


Figure 7. Micrographs of the API 5L X52 steel surface: a) before immersion in 0.5 M H₂SO₄ and b) after the attack in the corrosive medium without CI

Figure 8 (a) shows clearly the flow pattern on the steel surface, formed by the momentum exerted by the angular velocity whose strength produced the accumulation of corrosion products and CI molecules (TAA). Similar observations regarding the flux influence on the formation of corrosion products have been reported [38]. The zone framed with the red rectangle in Figure 8 (a) is shown in Figure 8 (b), observing two zones: one with accumulation of corrosion products and the other one free of them. Figure 8 (c) shows the magnification of the blue rectangle in Figure 8 (b), which confirms the evident protection provided by TAA due to the similar characteristics kept by the surface in Figure 7 (a), nonetheless, a slight presence of corrosion products is observed, which is due to the IE_T of 74 %.

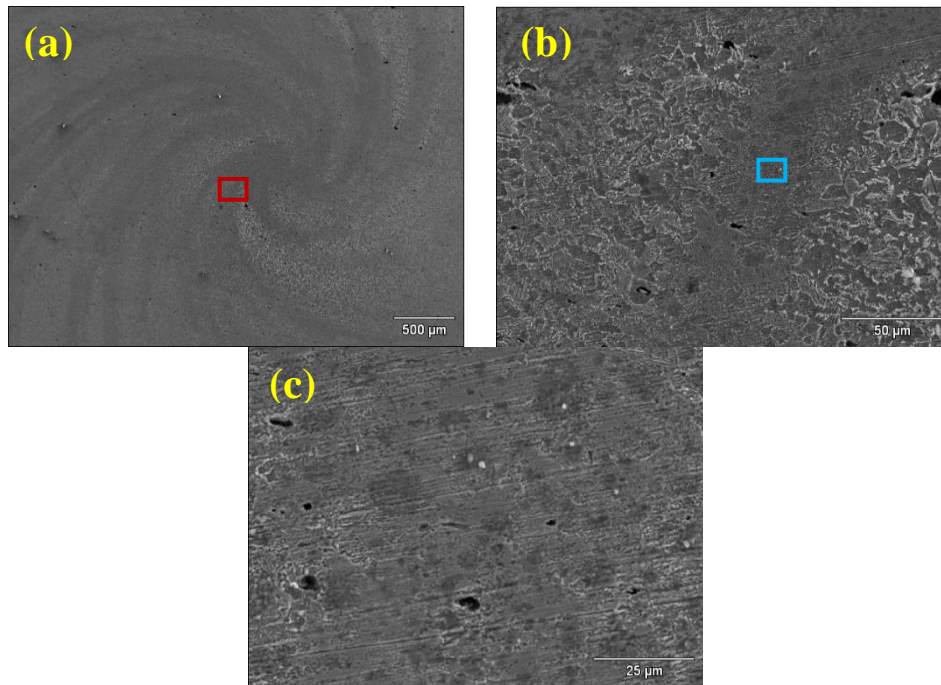
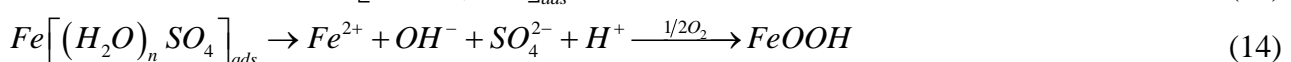
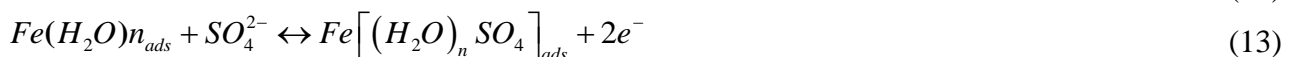
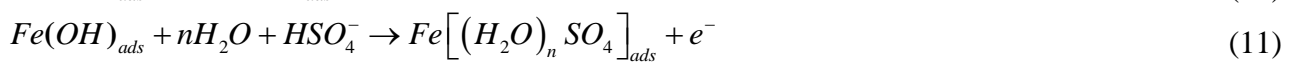


Figure 8. Micrographs of the steel surface after 2 h in 0.5 M H₂SO₄ in the presence of TAA at 100 ppm and $N_{Re} = 4500$

3.4. Inhibition mechanism

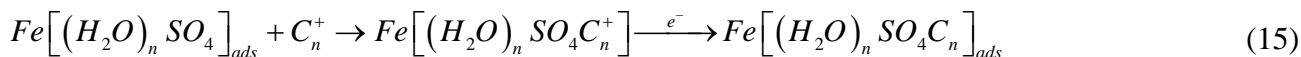
3.4.1. Anode reactions

On the anodic sites, the oxidation reactions can occur with and without the presence of CI with the corresponding steel dissolution that not only depends on the OH^- ions, but also on HSO_4^- and SO_4^{2-} [39]. However, the oxidation process of API 5L X52 steel in aqueous medium has its initial stage with the adsorption of water molecules on metal active sites according to the following reactions [40]:



Iron hydroxide, $Fe(OH)_{ads}$, is unstable and can react with bisulfates (Reactions 11 and 12), forming iron sulfates; in the absence of CI, the formed iron sulfates can undergo oxidation by dissolved oxygen, favoring the formation of iron oxyhydroxides (Reaction 14). As iron sulfates are slightly soluble in aqueous medium, they can be adhered to the steel surface, covering the metal surface; if the formed layer is highly porous, it will eventually be detached from the surface, allowing its interaction with hydronium ions and water molecules. Furthermore, the agglomeration of corrosion products and the

shear stress make difficult the interaction between the CI molecules and the active sites, thus affecting the IE of the CIs in this medium [41]. According to the chemical structure of the ILs, the adsorption process can be described by chemical and physical adsorption based on the following reactions:



where C_n^+ and φ^- are the cation and the anion, respectively.

From the electrochemical and adsorption results, it can be established that the adsorption of CI occurs on the anodic sites. As the concentration of HSO_4^- and SO_4^{2-} ions is higher than that of the CI in the active zones, the dissolution of steel will occur, but the presence of the CIs diminishes this phenomenon. The CIs can be adsorbed on the anodic sites through chemical and physical bonds with the anions of the ILs (Reactions 17 and 18), competing with water, sulfate and bisulfate molecules. Characteristics of the CIs such as geometrical size, charge density and steric hindrance of the CI molecules play a major role in the adsorption process; for example, at stationary state, the IL with oleate as anion (TAO) displayed the highest IE with respect to those featuring laurate (TAL) and (TAA) anthranilate as anions due to the fact that it has a long alkyl chain (C17) that can form a hydrophobic layer oriented toward the solution, retarding the transfer of HSO_4^- and SO_4^{2-} ions toward the surface. In addition, TAO displays a double chemical bond that could favor the donation of an electron pair to the metal surface, thus promoting a chemisorption process. Furthermore, the quaternary-ammonium derived cation of the ILs can interact with the sulfate ions adsorbed on the steel surface through electrostatic attraction forces, reducing the corrosion rate of API 5L X52 steel [39] according to Reactions 15 and 16.

3.4.2. Cathode reactions

The adsorption process that governs this zone is mainly promoted by hydronium ion reactions and the evolution of gaseous hydrogen according to the following reactions:



The hydrogen evolution reaction proceeds through various stages, including the recombination and electrochemical desorption of protons (Reactions 21 and 22). Likewise, the CI cations can be adsorbed through an electrostatic way according to the following reactions:



The electrochemical results indicate a surface blockage in the cathodic zones, notwithstanding, the covered surface degree reached by the ILs ranges from 0.06 to 0.78, indicating the existence of uninhibited active sites, which could be due to the cation nature [42]. It has been reported that quaternary ammonium derivatives with alkyl chains with less than four carbon atoms exert steric effects on the molecule, thus limiting the adsorption of the triethylmethylammonium cation in the ILs [43].

Due to the contribution of the CIs to the redox reactions, the chemical structure of the ILs plays a major role in the donation of free electrons, which can favor the chemisorption process through the retro-donation mechanism.

4. CONCLUSIONS

The R_p and Tafel electrochemical results confirmed that the IE of the ILs was directly proportional to their concentration, obtaining the maximal IE s at 100 ppm with all the compounds at stationary and dynamic states. At transitory state, it was confirmed that at $N_{Re} = 4500$, the adsorption of TAL and TAA was favored due to the fluid momentum transfer toward the steel surface, giving as a result a higher adsorption of the CI molecule on the active sites. The analysis of the E_{corr} data confirmed that the novel ILs can be classified as mixed-type CIs and that their adsorption is due to physical and chemical processes. Then, the chemical structure of the anion in the evaluated ILs plays a key role in their performance as CIs in 0.5 M H_2SO_4 .

Finally, the SEM surface analyses showed adsorption patterns of the corrosion products, but likewise, they confirmed the surface protection by the presence of CIs.

ACKNOWLEDGEMENTS

The authors thankfully acknowledge the SNI. OOX and PAL thank BUAP-VIEP.

References

1. M. Finšgar, J. Jackson, *Corros. Sci.*, 86 (2014) 17.
2. H. Mohammed, S. b. Sobri, *Mater. Lett.*, 229 (2018) 82.
3. S. K. Saha, M. Murmu, N. C. Murmu, I. B. Obot, P. Banerjee, *Surf. Interfaces*, 10 (2018) 65.
4. M. Askari, M. Aliofkhaezai, S. Ghaffari, A. Hajizadeh, *J. Nat. Gas Sci. Eng.*, 58 (2018) 92.
5. M. A. Dar, *Ind. Lubr. Tribol.*, 63 (2011) 227.
6. P. B. Raja, M. G. Sethuraman, *Mater. Lett.*, 62 (2008) 113.
7. M. M. Solomon, S. A. Umoren, I. B. Obot, A. A. Sorour, H. Gerengi, *ACS Appl. Mater. Interfaces*, 10 (2018) 28112.
8. C. Verma, I. B. Obot, I. Bahadur, E.-S. M. Sherif, E. E. Ebenso, *Appl. Surf. Sci.*, 457 (2018) 134.
9. R. Dong, P. Wen, S. Zhang, C. Zhang, W. Sun, M. Fan, D. Yang, F. Zhou, W. Liu, *Tribol. Int.*, 114 (2017) 132.
10. M. Goyal, H. Vashisht, S. Kumar, I. Bahadur, *J. Mol. Liq.*, 261 (2018) 162.
11. K. Zhang, W. Yang, Y. Chen, B. Xu, X. Yin, Y. Liu, H. Zuo, *J. Mater. Sci.*, 53 (2018) 14666.
12. L. Feng, S. Zhang, Y. Qiang, S. Xu, B. Tan, S. Chen, *Mater. Chem. Phys.*, 215 (2018) 229.
13. X. W. Zheng, S. T. Zhang, W. P. Li, M. Gong, L. L. Yin, *Corros. Sci.*, 95 (2015) 168.
14. C. Gabler, C. Tomastik, J. Brenner, L. Pizarova, N. Doerr, G. Allmaier, *Green Chem.*, 13 (2011) 2869.
15. H. Lgaz, A. Anejjar, R. Salghi, S. Jodeh, M. Zougagh, I. Warad, M. Larouj, P. Sims, *Int. J. Corros. Scale Inhib.*, 5 (2016) 209.
16. M. R. Ortega Vega, S. R. Kunst, J. A. T. da Silva, S. Mattedi, C. de Fraga Malfatti, *Corros. Eng.*,

- Sci. Technol.*, 50 (2015) 547.
17. S. Kumar, M. Goyal, H. Vashisht, V. Sharma, I. Bahadur, E. E. Ebenso, *RSC Adv.*, 7 (2017) 31907.
 18. P. Arellanes-Lozada, O. Olivares-Xometl, N. V. Likhanova, I. V. Lijanova, J. R. Vargas-Garcia, R. E. Hernandez-Ramirez, *J. Mol. Liq.*, 265 (2018) 151.
 19. J. Wysocka, M. Cieslik, S. Krakowiak, J. Ryl, *Electrochim. Acta*, 289 (2018) 175.
 20. M. N. Moussa, M. M. El-Tagoury, A. A. Radi, S. M. Hassan, *Anti-Corros. Methods Mater.*, 37 (1990) 4.
 21. M. El Azzouzi, A. Aouniti, M. El Massaoudi, S. Radi, B. Hammouti, M. A. Quraishi, H. Bendaif, Y. El Ouadi, *Int. J. Corros. Scale Inhib.*, 6 (2017) 463.
 22. ASTM (2011) G01-03-Standard Practice for Preparing, Cleaning, and Evaluating Corrosion Test Specimens. United States.
 23. ASTM (2004) G31-72. Standard Practice for Laboratory Immersion Corrosion Testing of Metals. United States.
 24. Y. Utanohara, M. Murase, *Nucl. Eng. Des.*, 342 (2019) 20.
 25. Y. Xu, M. Y. Tan, *Corros. Sci.*, 139 (2018) 438.
 26. S. Taguchi, Y. Ikarashi, T. Yamagata, N. Fujisawa, F. Inada, *Int. Commun. Heat Mass Transfer*, 90 (2018) 103.
 27. P. Madasamy, T. V. Krishna Mohan, A. Sylvanus, E. Natarajan, H. P. Rani, S. Velmurugan, *Eng. Failure Anal.*, 94 (2018) 458.
 28. M. Rosales, T. Pérez, J. L. Nava, *Electrochim. Acta*, 194 (2016) 338.
 29. M. J. Bahrami, S. M. A. Hosseini, P. Pilvar, *Corros. Sci.*, 52 (2010) 2793.
 30. M. T. Montañés, R. Sánchez-Tovar, J. García-Antón, V. Pérez-Herranz, *Corros. Sci.*, 51 (2009) 2733.
 31. N. C. Ngobiri, E. E. Oguzie, Y. Li, L. Liu, N. C. Oforika, O. Akaranta, *Int. J. Corros.*, 2015 (2015) 9.
 32. S. Bouakkaz, R. Zerdoumi, K. Oulmi, D. Mellahi, G. M. Andreadis, *Port. Electrochim. Acta*, 35 (2017) 211.
 33. M. Rbaa, F. Benhiba, I. B. Obot, H. Oudda, I. Warad, B. Lakhrissi, A. Zarrouk, *J. Mol. Liq.*, 276 (2019) 120.
 34. A. Q. Liu, C. Bian, Z. M. Wang, X. Han, J. Zhang, *Corros. Sci.*, 134 (2018) 149.
 35. T. Laabaissi, M. Rbaa, K. Ourrak, H. Zarrok, M. E. Faydy, B. Lakhrissi, H. Lgaz, R. Touri, I. Warad, H. Oudda, *J. Mater. Environ. Sci.*, 9 (2018) 1796.
 36. U. Schwertmann, R. M. Cornell, *Iron Oxides in the Laboratory: Preparation and Characterization*. WILEY-VCH, (2007) New York, USA.
 37. I. Lozano, E. Mazario, C. O. Olivares-Xometl, N. V. Likhanova, P. Herrasti, *Mater. Chem. Phys.*, 147 (2014) 191.
 38. J. Aguirre, M. Walczak, *Tribol. Int.*, 126 (2018) 177.
 39. O. Olivares-Xometl, E. Álvarez-Álvarez, N. V. Likhanova, I. V. Lijanova, R. E. Hernández-Ramírez, P. Arellanes-Lozada, J. L. Varela-Caselis, *J. Adhes. Sci. Technol.*, 32 (2018) 1092.
 40. O. Olivares-Xometl, N. V. Likhanova, N. Nava, A. C. Prieto, I. V. Lijanova, A. Escobedo-Morales, C. López-Aguilar, *Int. J. Electrochem. Sci.*, 8 (2013) 735.
 41. A. Pourghasemi Hanza, R. Naderi, E. Kowsari, M. Sayebani, *Corros. Sci.*, 107 (2016) 96.
 42. X. Zheng, S. Zhang, M. Gong, W. Li, *Ind. Eng. Chem. Res.*, 53 (2014) 16349.
 43. M. Drew, *Surfaces, Interfaces, and Colloids: Principles and Applications*. John Wiley & Sons, Inc.,